DOI 10.1007/s10812-018-0633-5
Journal of Applied Spectroscopy, Vol. 85, No. 2, May, 2018 (Russian Original Vol. 85, No. 2, March–April, 2018)

SPECTRAL ANALYSIS OF 3-(ADAMANTAN-1-YL)-4-ETHYL-1-[(4-PHENYLPIPERAZIN-1-YL) METHYL]-1*H*-1,2,4-TRIAZOLE-5(4*H*)-THIONE

Y. L. Mindarava,[a] M. B. Shundalau,[a,b*] L. H. Al-Wahaibi,[c] A. A. El-Emam,[d] A. S. Matsukovich,[e] and S. V. Gaponenko[a,e]

UDC 539.19;535.34;535.375.5

Vibrational IR (3200–650 cm^{-1}) and Raman spectra (3200–150 cm^{-1}) of adamantane-containing 3-(adamantan-1-yl)-4-ethyl-1-[(4-phenylpiperazin-1-yl)methyl]-1H-1,2,4-triazole-5(4H)-thione, which is promising for drug design, were examined. The UV/Vis spectrum (450–200 nm) of the compound in EtOH was measured. Full geometry optimization using density functional theory (DFT) in the B3LYP/cc-pVDZ approximation allowed the equilibrium configuration of the molecule to be determined and IR and Raman spectra to be calculated. Based on these, the experimental vibrational IR and Raman spectra were interpreted and the biological activity indices were predicted. The UV/Vis spectrum of the title compound was simulated at the time-dependent DFT/CAM-B3LYP/cc-pVDZ level with and without solvent effects and at the ab initio multi-reference perturbation theory XMCQDPT2 level. The UV/Vis spectrum that was simulated using the multi-reference XMCQDPT2 approximation agreed very successfully with the experimental data, in contrast to the single-reference DFT method. This was probably a consequence of intramolecular charge transfer.

Keywords: *3-(adamantan-1-yl)-4-ethyl-1-[(4-phenylpiperazin-1-yl)methyl]-1H-1,2,4-triazole-5(4H)-thione, FTIR spectrum, Raman spectrum, UV/Vis spectrum, density functional theory, multi-reference perturbation theory, biological activity.*

Introduction. Diamondoids (including adamantane as the simplest representative of the family) and their derivatives are viable candidates for drug development and delivery systems [1–3]. An adamantane motif in organic compounds increases their biological activity by increasing the lipophilicity and facilitating more efficient transport across biological membranes. Adamantane derivatives exhibit antiviral activity against influenza virus [4–6] and HIV [7–9] and possess antimicrobial [10–15], anti-inflammatory [15–17], and antiproliferative activity [18].

The present work studied the spectral characteristics of 3-(adamantan-1-yl)-4-ethyl-1-[(4-phenylpiperazin-1-yl) methyl]-1*H*-1,2,4-triazole-5(4*H*)-thione ($C_{25}H_{35}N_5S$) using experimental spectral (vibrational and electronic absorption) and theoretical methods (density functional theory, *ab initio* multi-reference perturbation theory). The adamantane derivative was recently synthesized and characterized by a single-crystal x-ray structure analysis [19].

Previously, quantum-chemical calculations determined the spectral characteristics of several adamantane derivatives of interest for drug synthesis, i.e., *N*′-(adamantan-2-ylidene)benzohydrazide [20, 21], 3-(adamantan-1-yl)-1-[(4-benzylpiperazin-1-yl)methyl]-4-phenyl-1*H*-1,2,4-triazole-5(4*H*)-thione [22], and 3-(adamantan-1-yl)-4-phenyl-1-[(4-phenylpiperazin-1-yl) methyl]-1*H*-1,2,4-triazole-5(4*H*)-thione [22]. The results of the present research may be useful in medicinal chemistry for new drug discovery owing to the interest in the pharmacological and structural properties of adamantane derivatives.

Experimental. IR absorption spectra (3200–650 cm^{-1}) were recorded using a Nexus FT-IR spectrometer (Thermo Nicolet, USA) equipped with a Continuum IR microscope (Thermo Fisher Scientific, USA) with a 15× objective (2 cm^{-1}

*To whom correspondence should be addressed.

[a]Belarusian State University, 4 Nezavisimost′ Ave., Minsk, 220030, Belarus; email: shundalov@bsu.by; [b]A. N. Sevchenko Institute of Applied Physical Problems, Belarusian State University, Minsk, Belarus; [c]College of Sciences, Princess Nourah Bint Abdulrahman University, Riyadh 11671, Saudi Arabia; [d]College of Pharmacy, King Saud University, Riyadh 11451, Saudi Arabia; [e]B. I. Stepanov Institute of Physics of the National Academy of Sciences of Belarus, Minsk, Belarus. Translated from Zhurnal Prikladnoi Spektroskopii, Vol. 85, No. 2, pp. 181–193, March–April, 2018. Original article submitted October 27, 2017.

resolution). Samples were prepared by grinding crystals into a powder that was spread into a thin film on the reflecting surface of the substrate (Al foil). The obtained signal was both scattered radiation from the sample and radiation that passed through the sample and was reflected from the substrate surface. Raman spectra (3200–150 cm^{-1}) were recorded using a continuous DPSS laser (λ = 532 nm, power 7 mW) as the excitation source. The angle between the excitation and recorded signal directions was 180^o. The recording system consisted of a Solar TII S3901 spectrograph equipped with a diffraction grating (1200 lines/mm) and CCD array (Princeton Instruments) cooled by liquid N_2. The signal accumulation time was 60 s. Electronic absorption spectra (450–200 nm) of the compound in EtOH were recorded using a Cary 500 spectrophotometer. The solvent effect was minimized by placing a cuvette with EtOH in the reference channel.

Structures and vibrational spectra of the compound were calculated using the GAMESS-US quantum-chemical suite [23]. Results were illustrated using MacMolPlt [24] and ORTEP [25] programs. Density functional theory (DFT) with a Dunning correlation-consistent, polarized valence, double-zeta basis set [26] and hybrid exchange-correlated functional B3LYP [27–29] was used to optimize the equilibrium structure and to calculate the Hessian (force field), eigenfrequencies of modes in the harmonic approximation, and IR and Raman intensities.

Calculations in the first stage searched for a stable configuration using gradient optimization of all molecular geometric parameters. When the optimization was completed, the eigenfrequencies of modes in the harmonic approximation and intensities in IR and Raman vibrational spectra were calculated. The force field was computed considering two shifts (in positive and negative directions) of each atom relative to its equilibrium position along each of three Cartesian axes. This approach improved by 20–50 cm^{-1} (or ~1%) the accuracy of the calculated vibrational frequencies. In several instances, imaginary frequencies for low-frequency bending vibrations were avoided. The aforementioned improvement in the accuracy turned out to be very important because the harmonic frequencies of stretching modes of terminal groups that are calculated using the B3LYP/cc-pVDZ approximation are usually 4–5% greater than the experimental ones. The lack of imaginary frequencies in the calculated spectrum confirmed that the obtained structure was located at a minimum on the potential-energy surface. Vibrational bands and lines were assigned by calculating the potential-energy distribution over internal coordinates.

Time-dependent density functional theory (TDDFT) [30] is currently widely used to simulate electronic spectra of polyatomic molecular systems. Quantum-chemical calculations using the TDDFT formalism with the local spin density approximated by gradient corrections (i.e., using standard exchange-correlation functionals, e.g., hybrid functional B3LYP) are known to give deviations up to 0.4 eV for the energies of the lower excited states from the experimental ones [31]. This is especially typical of molecular systems with charge transfer. Phenyl, piperazine, and triazole groups in the studied molecule allowed it to be classified as a molecular system that could exhibit intramolecular charge transfer (ICT). The Coulomb-attenuating method (CAM) approximation (or refined LRC method) that was developed for such instances [32] could sometimes improve the qualitative and quantitative calculations. Thus, the spectral and energy characteristics of the excited singlet states of the studied compound were calculated using the TDDFT method with cc-pVDZ basis set [26] and hybrid functional CAM-B3LYP [32]. The solvent (EtOH) effect was accounted for in the solvation model density (SMD) approximation [33]. The quantum-chemical GAMESS-US suite was also used for the calculations.

Multi-reference approximations (e.g., the *ab initio* multi-reference perturbation theory method) are alternatives to the TDDFT method. Our recent work [21] demonstrated that *ab initio* calculations in the multi-reference approximation CASSCF/XMCQDPT2 [34] explained very successfully the electronic absorption spectrum of *N*′-(adamantan-2-ylidene) benzohydrazide considering the presence of four conformers in solution [21].

The electronic absorption spectrum of the studied molecule was calculated in the CASSCF/XMCQDPT2 approximation using the Firefly quantum-chemical suite [35] and standard basis set cc-pVDZ [26]. The first stage included CASSCF calculations with the density-matrix averaged over seven states (four singlets and three triplets) for two active electrons involving four active orbitals. Then, calculations used the XMCQDPT2 approximation [34]. The electronic correlation energy for all 117 doubly occupied orbitals in the ground configuration was taken into account. The energy denominator shift (EDS) was 0.01.

The structure determination of the studied molecule enabled calculation of its biological activity indices (probability to be active/inactive, *Pa*/*Pi*), i.e., the probability that biological activity of a particular type was present (absent). The biological activities were obtained using the PASS database [36], the online version of which [37] predicted greater than 4,000 different biological activities based only on the compound structural data.

Results and Discussion. Figure 1 shows the equilibrium structure of the studied molecule. The molecule of 3-(adamantan-1-yl)-4-ethyl-1-[(4-phenylpiperazin-1-yl)methyl]-1*H*-1,2,4-triazole-5(4*H*)-thione contained the functional groups adamantyl (A), phenyl (Ph), piperazine (P), and triazole rings (T) and methyl (M) and ethyl (Et). Several of them

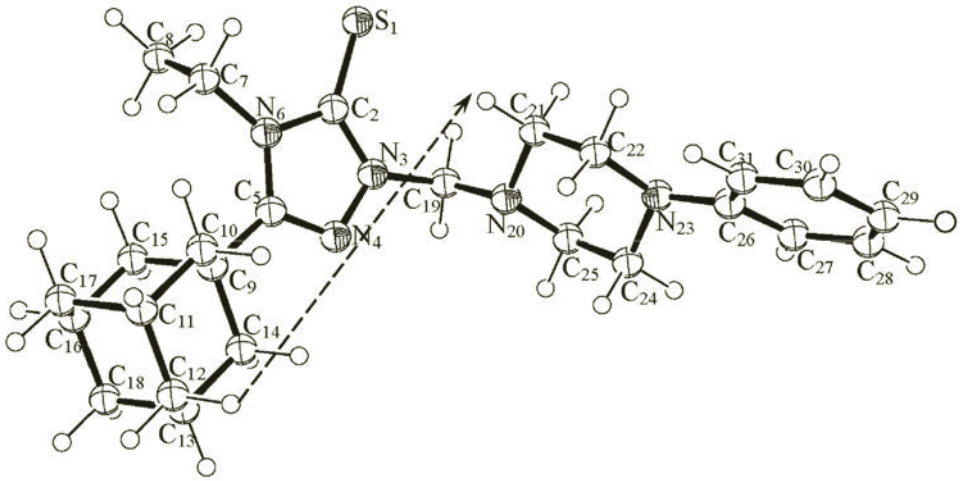

Fig. 1. Equilibrium structure and electric dipole moment of 3-(adamantan-1-yl)-4-ethyl-1-[(4-phenylpiperazin-1-yl)methyl]-1*H*-1,2,4-triazole-5(4*H*)-thione calculated in the B3LYP/cc-pVDZ approximation.

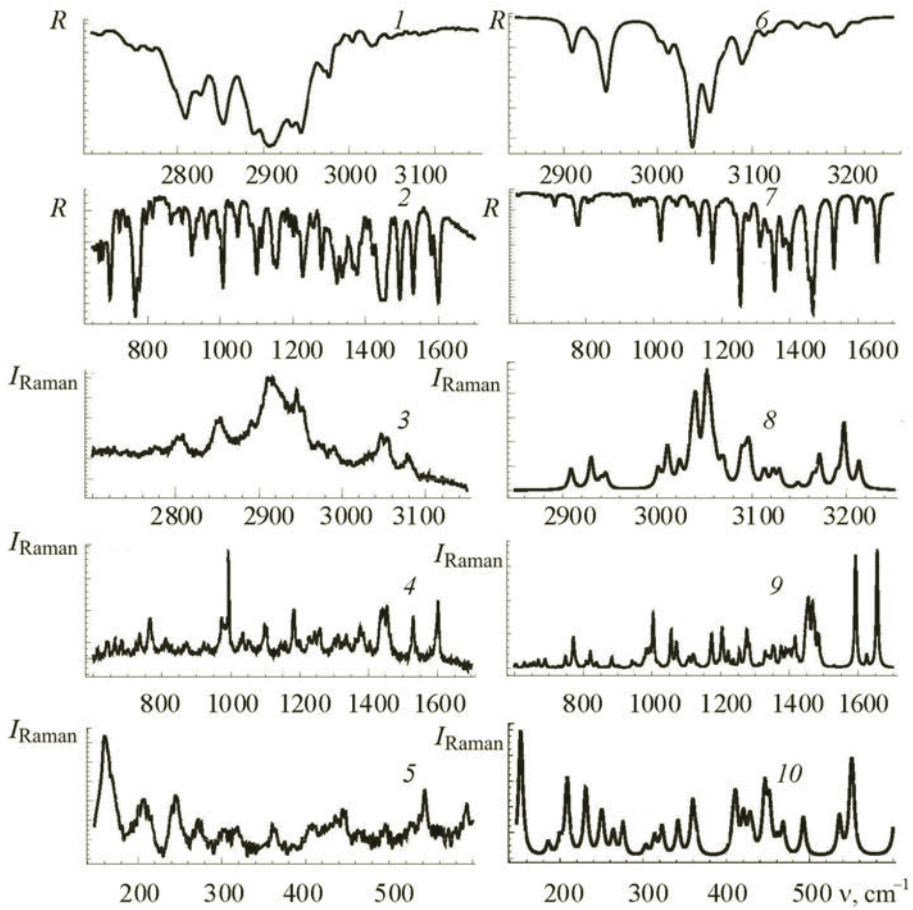

Fig. 2. Experimental (1–5) and calculated (B3LYP/cc-pVDZ) (6-10) IR (1, 2, 6, 7) and Raman spectra (3-5, 8-10) of 3-(adamantan-1-yl)-4-ethyl-1-[(4-phenylpiperazin-1-yl) methyl]-1*H*-1,2,4-triazole-5(4*H*)-thione.

TABLE 1. Frequencies (cm^{-1}) and Intensities in Experimental and Calculated IR and Raman Spectra of 3-(Adamantan-1-yl)-4-ethyl-1-[(4-phenylpiperazin-1-yl)methyl]-1*H*-1,2,4-triazole-5(4*H*)-thione

ν_{IR}^{exp}	ν_{Raman}^{exp}	ν^{calc}	I_{IR}^{calc}	I_{Raman}^{calc}	Assignment
	3080 w	3213	0.04	0.34	νCH(Ph)
	3055 m	3197	0.10	0.85	νCH(Ph)
3047 vw	3047 m	3190	0.17	0.15	νCH(Ph)
3028 w		3172	0.06	0.42	νCH(Ph)
3003 vw		3165	0.04	0.15	νCH(Ph)
2986 sh	2989 w				2×1495
2977 m		3149	0.09	0.07	$\nu CH_3 + \nu CH_2$(Et)
2971 m	2970 w	3129	0.00	0.23	$\nu CH_3 + \nu CH_2$(Et)
		3122	0.09	0.22	νCH(P)
		3113	0.12	0.24	νCH_3
	2953 s	3098	0.08	0.17	νCH_2(M)
		3096	0.06	0.38	νCH(P)
		3093	0.09	0.21	νCH(P)
		3089	0.15	0.26	νCH_2(A)
		3088	0.19	0.14	νCH_2(A)
2943 vs	2941 vs	3070	0.13	0.20	νCH_2(A)
2934 vs		3068	0.08	0.17	νCH_2(A) + νCH_2(M)
		3061	0.17	0.27	νCH(P)
		3056	0.56	0.63	νCH_2(A)
	2917 vs	3052	0.20	1.00	νCH_2(A) + νCH(A)
		3051	0.10	0.13	νCH_2(A)
		3049	0.04	0.24	νCH_2(A)
2911 vs		3041	0.32	0.79	νCH_2(A) + νCH(A)
		3038	0.19	0.41	νCH_3(M)
2907 vs	2909 vs	3037	0.55	0.15	νCH_2(A) + νCH(A)
		3035	0.37	0.23	νCH_2(A) + νCH(A)
		3025	0.19	0.09	νCH_2(A) + νCH(A)
2888 vs	2889 m	3023	0.02	0.21	νCH_2(A) + νCH(A)
		3012	0.10	0.19	νCH_2(A) + νCH(A)
2853 s	2855 m	3011	0.09	0.16	νCH_2(A) + νCH(A)
	2847 m	3010	0.07	0.20	νCH_2(A) + νCH(A)
		3001	0.14	0.25	νCH_2(M)
		2945	0.66	0.19	νCH(P) + νCH_2(P)
2826 m		2940	0.21	0.10	νCH(P) + νCH_2(P)
		2930	0.08	0.40	νCH(P) + νCH_2(P)
		2909	0.34	0.27	νCH(P)
2809 s	2809 w				1450 + 1362
2795 sh	2802 w				1441 + 1361
					1418 + 1377
	2776 vw				1404 + 1374
2769 w					1579 + 1190
2751 w					1472 + 1279

TABLE 1. (Continued)

ν_{IR}^{exp}	ν_{Raman}^{exp}	ν^{calc}	I_{IR}^{calc}	I_{Raman}^{calc}	Assignment
1599 vs	1602 s	1655	0.63	0.28	νCC(Ph) + δ(i.p.)CCC(Ph)
1579 m		1624	0.06	0.03	νCC(Ph) + δ(i.p.)CCC(Ph)
1533 vs	1529 m	1592	0.26	0.27	νCN(T)
1495 vs		1529	0.66	0.00	νCC(Ph) + δ(i.p.)CCC(Ph)
1472 w		1493	0.01	0.01	σCH_2(A)
		1486	0.04	0.05	σCH_2(P) + σCH_2(M)
1450 vs	1453 m	1483	0.00	0.01	νCC(Ph) + δ(i.p.)CCC(Ph)
		1482	0.02	0.02	σCH_2(A) + σCH_2(M)
		1474	0.21	0.04	σCH_2(P)
1442 vs	1441 m	1472	0.02	0.04	σCH_2(A)
		1468	0.66	0.10	σCH_2(M) + νCN(T)
		1466	0.01	0.01	σCH_2(A)
1418 m		1465	0.26	0.01	σCH_2(A) + σCH_2(M) + σCH_3(M)
		1460	0.01	0.02	νCN(T) + σCH_2(M) + σCH_2(P)
1404 w	1404 vw	1459	0.11	0.02	σCH_2(M) + σCH_2(P)
		1457	0.15	0.04	νCN(T) + σCH_2(M)
		1455	0.30	0.08	σCH_2(A) + σCH_2(M)
		1451	0.05	0.05	σCH_2(A)
		1449	0.13	0.04	σCH_2(P) + σCH_2(M) + νCN(T)
		1445	0.01	0.04	σCH_2(A)+ σCH_2(M)
1383 sh	1384 w	1426	0.05	0.01	νCC(P) + σCH_2(M) + σCH_2(P)
		1417	0.07	0.06	νCN(T) + σCH_2(M)
1377 s	1374 w	1410	0.09	0.03	σCH_2(P) + σCH_2(M)
		1401	0.54	0.03	νCN(T) + σCH_2(M)
		1397	0.05	0.02	νCC(M) + σCH_2(M)
		1395	0.03	0.01	νCC(A) + σC_2H(A)
		1391	0.01	0.01	νCC(A) + σC_2H(A)
1362 s	1361 sh	1390	0.20	0.02	ωCH_2(M) + ωCH_2(P)
		1385	0.04	0.01	ωCH_2(A)
1356 sh		1380	0.33	0.01	νCN(T) + ωCH_2(M) + ωCH_3(M)
1344 sh		1376	0.00	0.04	ωCHN(P)
		1374	0.00	0.00	ωCH_2(A)
		1372	0.01	0.00	ωCH_2(A)
		1363	0.03	0.00	νCC(Ph) + ωCH_2(P)
1335 s	1338 vs	1355	0.64	0.03	νC(M)N(T) + σCNN(T)
		1351	0.25	0.03	νCC(Ph) + ωCH_2(P)
		1348	0.07	0.01	νCC(A)
1321		1343	0.02	0.00	ωCH_2(P)
		1340	0.05	0.01	ωCH_2(A)
		1338	0.01	0.01	νCC(Ph) + νCN(P)
	1311 vs	1337	0.05	0.00	νCC(A) + ωCH_2(A)
1296 w	1301 vs	1334	0.13	0.01	νCN(T) + νCN(P)
		1328	0.09	0.03	σNCH(P)
		1317	0.18	0.00	νCN(T) + νCC(A)
1279 m		1314	0.01	0.00	νCC(A) + γCH_2(A)

TABLE 1. (Continued)

ν_{IR}^{exp}	ν_{Raman}^{exp}	ν^{calc}	I_{IR}^{calc}	I_{Raman}^{calc}	Assignment
		1312	0.00	0.00	νCC(A)
		1310	0.36	0.01	γCH_2(M) + νCN(T) + νCN(P)
1254 w	1257 w	1282	0.10	0.04	νCN(T) + νCS + νCC(A)
		1277	0.12	0.02	νCC(A) + γCH_2(M)
		1275	0.01	0.06	γCH_2(A)
		1270	0.02	0.02	σNCN(T)
	1243 w	1254	1.00	0.04	νCC(Ph) + νCN(P)
1224 s	1225 vw	1235	0.11	0.02	ωCH_2(M) + ωCH_2(P)
1211 sh		1221	0.03	0.03	ωCH_2(P)
1201 w		1205	0.01	0.05	γCH_2(A)
1190 w		1202	0.00	0.05	γCH_2(A)
		1201	0.02	0.02	ωCCH(Ph)
1176 w	1178 m	1191	0.06	0.01	νCN(T) + νCN(P)
1153 s	1156 vw	1174	0.16	0.03	νCN(P)
1147 s	1143 vw	1172	0.46	0.04	νC(M)N(P)
		1170	0.01	0.02	ωCCH(Ph)
		1138	0.00	0.00	ωCH_2(A)
		1134	0.35	0.00	νCN(T) + ωCH_2(M)
		1130	0.01	0.00	γCH_2(A)
		1124	0.04	0.01	ρCH_2(A)
1109 m		1120	0.02	0.02	ρCH_2(A)
		1118	0.01	0.01	ρCH_2(A)
1100 s	1099 m	1108	0.07	0.02	νCN(P)
		1106	0.02	0.00	νCC(Ph)
1084 sh		1102	0.02	0.01	ωCH_2(M)
		1079	0.01	0.01	ωCH_2(P)
		1072	0.00	0.04	ωCH_2(P)
		1070	0.05	0.02	νCN(T) + νCN(P)
1048	1051 vw	1066	0.06	0.00	νCN(T) + νCC(A)
1043 sh		1057	0.00	0.00	νCC(A)
	1034w.	1055	0.04	0.08	νCC(Ph)
		1054	0.00	0.00	νCC(A)
1026 vw		1052	0.00	0.00	νCC(A)
1006 s		1021	0.39	0.01	νCN(P) + ωCH_2(M)
		1015	0.08	0.00	νCN(T) + ωCH_2(M)
996 m	993 vs	1003	0.01	0.12	δCCC(Ph)
983 vw		994	0.01	0.00	νCC(Ph) + νCH(Ph)
		994	0.02	0.03	νCC(A)
		986	0.00	0.03	νCC(A)
		983	0.00	0.02	νCC(A)
		977	0.05	0.01	νCN(T) + ωCH_2(M)
963 m	966 m	973	0.00	0.00	νCC(Ph) + νCH(Ph)
		961	0.09	0.00	νCN(P) + ωCH_2(M)

TABLE 1. (Continued)

ν_{IR}^{exp}	ν_{Raman}^{exp}	ν^{calc}	I_{IR}^{calc}	I_{Raman}^{calc}	Assignment
943 w		951	0.00	0.01	νCC(A)
934 m	934 vw	948	0.00	0.00	νCC(A)
923 m	921 vw	943	0.11	0.01	νCC(Ph) + νCN(P)
897 w		900	0.02	0.00	νCC(Ph) + νCH(Ph)
		896	0.00	0.00	ρCH_2(A)
		890	0.00	0.00	ρCH_2(A)
		884	0.00	0.00	ρCH_2(A)
865 w	868 vw	881	0.03	0.02	νCC(A)
		861	0.01	0.00	ρCH_2(P)
		837	0.01	0.01	ρCH(Ph)
		827	0.00	0.00	νCC(A)
813 w	809 vw	824	0.01	0.00	νCC(A)
		819	0.05	0.04	νCN(P) + νC(M)N(P)
798 w		807	0.07	0.01	νC(M)N(T) + δ(o.o.p.)CNC(T)
779 s		779	0.21	0.00	ρCH_2(M)
766 vs	763 m	775	0.12	0.01	δ(o.o.p.)CH(Ph) + δCCC(A)
743 w		770	0.08	0.07	δCCC(A)
	734 w	747	0.02	0.03	δ(i.p.)CCC(Ph)
721 w		728	0.00	0.00	ωCN_2(T)
696 s	699 vw	710	0.12	0.00	δ(o.o.p.)CCC(Ph)
675 m	675 vw	688	0.01	0.02	δCCC(A) + ωCN_2(T)
		683	0.02	0.00	δ(o.o.p.)CNC(T)
663 m	661 vw	669	0.01	0.02	δ(o.o.p.)CNC(T)
	640 vw	656	0.00	0.00	δCCC(A)
		655	0.00	0.01	δCCC(A)
		645	0.00	0.01	δ(i.p.)CCC(Ph) + ρCH_2(P)
	614 vw	629	0.00	0.01	δ(i.p.)CCC(Ph)
	594 vw	604	0.02	0.01	δ(i.p.)CNC(T) + γCH_2(M)
	542 vw	551	0.03	0.01	νCS+ρCH_2(M) + ρCH_2(P)
		549	0.01	0.01	νCS+ρCH_2(M) + ρCH_2(P)
	525 vw	536	0.05	0.00	δ(i.p.)CCC(Ph) + ρCH_2(P)
	496 vw	493	0.00	0.00	δCNC(P)
	465 vw	468	0.01	0.00	δCCC(A)
		461	0.01	0.00	δCCC(A) + ωCN_2(T)
		451	0.00	0.01	δCCC(A) + δCNC(P)+δCH_2(M)
	444 vw	446	0.01	0.01	δCCC(A) + δCNC(P)+δCH_2(M)
		431	0.01	0.00	δCCC(A) + δCNC(T)
		428	0.01	0.00	δCNC(P) + δCH_2(M) + δCNC(T)
		420	0.01	0.00	δ(o.o.p.)CCC(Ph)
	409 vw	411	0.00	0.00	δCCC(A) + δCNC(P)
		411	0.00	0.00	δCCC(A) + δCNC(P)
		408	0.00	0.00	δCCC(A)
	362 vw	364	0.00	0.00	δCCC(A)

TABLE 1. (Continued)

ν_{IR}^{exp}	ν_{Raman}^{exp}	ν^{calc}	I_{IR}^{calc}	I_{Raman}^{calc}	Assignment
		359	0.02	0.01	δCCC(A) + δCNC(P) + δCH_2(M)
		342	0.02	0.00	δCCC(Ph) + δCNC(P) + δCH_2(M)
		323	0.03	0.00	δCNC(P)
	316 vw	317	0.00	0.00	δCCC(A)
	305 vw	314	0.00	0.00	δ(o.o.p.)CNC(T) + σHCC(M)
		303	0.00	0.00	δ(o.o.p.)CNC(T) + σHCC(M) + δCNC(P)
	272 vw	276	0.01	0.00	νCS + ρCH_2(P)+ δCCC(Ph)
		264	0.01	0.00	νCS + ρCH_2(M) +ρCH_2(P)
		250	0.01	0.00	ρCH_2(M) + ρCH_2(P)
	245 vw	248	0.01	0.00	ρCH_2(M) + ρCH_3(M)
		231	0.01	0.01	ρCSN(T) + ρCH_2(P) + δCCC(Ph)
	207 vw	209	0.01	0.01	ρCSN(T) + ρCH_2(P) + δCCC(Ph)
		200	0.00	0.00	ρCSN(T) + ρCH_2(P) + δCCC(Ph)+ δCCC(A)
	160 w	186	0.01	0.00	δCC(Et)N(T)

Note. Band and line intensities I_{IR} and I_{Raman} are normalized to the strongest band or line; vs, very strong; s, strong; m, medium; w, weak; vw, very weak; sh, shoulder; normal modes: ν, stretching; δ, bending; ρ, rocking; σ, scissoring; ω, wagging; γ, twisting; i.p., in-plane bending; o.o.p., out-of-plane bending vibrations.

(e.g., adamantyl, phenyl, or ethyl) possessed highly characteristic vibrational frequencies that, as a rule, did not mix with vibrations of other functional groups. The other fragments, e.g., triazole, methyl, and piperazine, could in several instances be considered a molecular framework so that the vibrations of these fragments mixed and were delocalized over the whole framework.

The calculated structural parameters of the isolated molecule gave deviations of ≤1% for most calculated bond lengths from the experimental ones. Only bonds involving the N atoms (i.e., C–N and N–N of the piperazine and triazole rings) had errors of ~2% for the calculated bond lengths. A similar situation was observed previously for *N*′-(adamantan-2-ylidene)benzohydrazide [21], 4,4′-methylenediphenyldiisocyanate [38], and benzohydrazide [39] and was most probably characteristic of the used combination of basis set and functional. An analogous tendency was found for the in-plane angles. Angles between C–N bonds typically had the greatest errors (up to 4%). In other instances, the deviations of the calculated values from the experimental ones were usually ≤1%. It is also noteworthy that the C–H bond lengths that were fixed in the x-ray structure analysis [19] at 0.97 Å (A, P, M), 0.96 (Et), and 0.93 (Ph) differed noticeably from the experimental values for adamantane (1.112 ± 0.004 Å [40]), phenol (1.080–1.086, average 1.083 Å [41]), piperazine (1.133 Å [42]), and methylene (1.085 Å [43]).

Figure 2 shows the experimental and calculated IR and Raman spectra of the studied compound. Table 1 presents experimental vibrational frequencies and those calculated at the B3LYP/cc-pVDZ level of theory and the corresponding intensities in the IR and Raman spectra. In most instances, the vibrations were localized on one of the functional groups (adamantyl, phenyl, ethyl, piperazine, methylene, or triazole).

Vibrations of the adamantyl fragment. Frequencies of CH- and CH_2-stretching vibrations in monosubstituted adamantyl lay in the range 2952–2850 cm^{-1} [44]. According to the literature [44] and our calculations [20, 22], bands at 2943, 2934, 2911, 2907, 2888, and 2953 cm^{-1} in the IR spectrum and lines at 2941, 2917, 2909, 2889, 2855, and 2847 cm^{-1} in the Raman spectrum belonged to adamantyl CH and CH_2 stretching vibrations. Adamantyl CH_2 scissoring vibrations were located at 1475–1440 cm^{-1} [44]. Monosubstitution lifted the degeneracy of CH_2 wagging vibrations (~1350 cm^{-1}) and led to the appearance of a specific sequence of bands in the range 1400–1300 cm^{-1} [45]. Thus, bands at ~1472 and 1441 cm^{-1} were assigned to scissoring vibrations of adamantane CH_2 groups; bands and lines at 1362, 1321, and 1311 cm^{-1}, to wagging vibrations. Furthermore, adamantyl vibrations appeared near 1200 (CH_2 twisting vibrations), 1100 (CH_2 rocking vibrations), 800 (CC stretching vibrations) and in the ranges 780–740 and 460–330 cm^{-1} (adamantyl CCC bending vibrations) [44, 45]. Thus, bands at 1201 and 1190 cm^{-1} corresponded to CH_2 twisting vibrations; bands and lines at 865 (IR), 868 (Raman),

813 (IR), and 809 cm^{-1} (Raman), to CC stretching vibrations; and 743 (IR), 640 (Raman), 465 (Raman), 362 (Raman) and 316 cm^{-1} (Raman), to CCC bending vibrations.

Vibrations of the phenyl group. Stretching vibrations of CH- and CC-bonds in aromatic compounds are usually found in the ranges 3100–3000 and 1630–1200 cm^{-1} [46]. Thus, the spectrum of benzene has bands at ~1596, 1486, and 1310 cm^{-1} [47]. This allowed us to assign the bands at 1599, 1579, 1495, and 1450 cm^{-1} in the IR spectrum and lines at 1602 and 1453 cm^{-1} in the Raman spectrum to phenyl-ring CC stretching vibrations. Strong IR bands at 996 and 969 cm^{-1} and a Raman line at 993 cm^{-1} were attributed to ring bending vibrations (1010 and 707 cm^{-1} in the spectrum of benzene [47]). In-plane and out-of-plane ring bending vibrations were also observed near 734 and 614 cm^{-1}.

Vibrations of ethyl and methyl groups. CH_2 and CH_3 stretching vibrations were observed at 2980–2950 cm^{-1} [46]. Bands at 2977 and 2971 cm^{-1} in the IR spectrum and lines at 2970 and 2953 cm^{-1} in the Raman spectrum were assigned to stretching vibrations of these groups. Twisting and wagging vibrations lay in the range 1370–1080 cm^{-1} [46]; scissoring and rocking vibrations, ~1080 and 780 cm^{-1} [46]. It is noteworthy that methylene vibrations were mixed with bending vibrations of triazole and piperazine rings linked to it.

Vibrations of the piperazine group. According to the literature [42, 48], CH_2 stretching vibrations in pure piperazine appeared at 3087, 2987, 2914, 2853, and 2750 (IR [42]); 2833 and 2771 (Raman [42]); and 2944 cm^{-1} (IR [48]). In our opinion, frequencies of 2750 and 2771 cm^{-1} are too low for CH_2 stretching vibrations and the aforementioned bands and lines were more likely combined frequencies or overtones (Table 1). Thus, the band at 2826 cm^{-1} in the IR spectrum of the studied molecule was assigned to piperazine-ring CH and CH_2 stretching vibrations. Scissoring and wagging CH_2 vibrations for pure piperazine [42, 48] and 1-phenylpiperazine [49] were observed at ~1458–1431 [48], 1426 [42], 1407 [49], 1390, 1364, 1360 [42], and 1190 cm^{-1} [49]. Bands and lines at 1377, 1321, and 1211 cm^{-1} were attributed to σCH_2- and ωCH_2 vibrations of the piperazine ring. Stretching vibrations of heteroaromatic rings were found to interact with each other [46]. Therefore, it was impossible to isolate vibrational frequencies of separate CC-, CN-, or NN-bonds. Stretching vibrations of heteroaromatic rings were observed at 1600–1300 cm^{-1} [46], i.e., in the same region as for aromatic rings, and were often masked by each other. Bands at 1177, 1115, and 933 cm^{-1} in the IR spectrum and lines at 1184, 1109, and 836 cm^{-1} in the Raman spectrum of pure piperazine were identified as belonging to ring vibrations [48]. Researchers also assigned bands and lines for pure piperazine at 1323 (IR), 1294 (Raman), 1268 (IR), 1218 (IR), 1173 (IR), 1120 (Raman), 1055 (IR), and 1049 cm^{-1} (Raman) to CN stretching vibrations; a band at 1199 cm^{-1} in the IR spectrum and a line at 1186 cm^{-1} in the Raman spectrum, to CC stretching vibrations [42]. Thus, according to the literature [42, 48] and our calculations, bands at 1153, 1100, and 1006 cm^{-1} in the IR spectrum and 1156 and 1099 cm^{-1} in the Raman spectrum were assigned to piperazine skeletal (CC and CN bonds) stretching vibrations. In-plane and out-of-plane piperazine-ring bending vibrations lay below 920 cm^{-1}. The corresponding spectral bands and lines were assigned based on our calculations.

Vibrations of the triazole ring. The situation was analogous for skeletal stretching vibrations of the triazole ring. CN, NN, and CS stretching vibrations coupled with each other. Their frequencies depended on the type of substitution. Breathing vibrations of the 1*H*-1,2,4-triazole ring were observed at ~1540 [50], 1495–1482 [50, 51], 1473 [50], 1390–1361 [50, 51], 1272–1255 [51], 1146 [51], 1190 [50], and 1062–1055 cm^{-1} [51]. Thus, bands and lines near 1533 (IR), 1529 (Raman), 1338 (Raman), 1335 (IR), 1257 (Raman), 1254 (IR), 1051 (Raman) and 1048 cm^{-1} (IR) belonged to triazole-ring breathing vibrations. Other triazole-ring bending vibrations lay below 800 cm^{-1}. The corresponding bands and lines were also assigned based on our calculations. Bands at 1418, 1383, 1356, 1296, 1224, 1176, and 1147 cm^{-1} in the IR spectrum and lines at 1384, 1301, 1243, 1225, 1178, and 1143 cm^{-1} in the Raman spectrum corresponded according to our calculations to stretching and bending vibrations delocalized over various functional groups of the molecular framework.

UV/Vis spectrum. Figure 3 (curve 1) shows the experimental electronic absorption spectrum of the studied compound dissolved in EtOH. The long-wavelength absorption band maximum was located at 252 nm. The possibility of a bathochromic shift of the band due to the influence of the polar solvent (EtOH) and the fact that the purely electronic 0–0-transition (the wavelength of which was also calculated quantum chemically) lay on the long-wavelength side of the absorption band had to be considered in order to compare correctly the quantum-chemically calculated and experimental electronic absorption spectra. On this basis, it could be assumed that the wavelength of the 0–0-transition of the pure compound should coincide approximately with the wavelength of the absorption-band maximum in EtOH, i.e., in the region 250–255 nm.

Figure 3 and Table 2 also show electronic absorption spectra calculated in the approximations TDDFT/CAM-B3LYP/cc-pVDZ, TDDFT/CAM-B3LYP/cc-pVDZ+SMD (EtOH), and CASSCF(2,4)/XMCQDPT2. These results indicated that the calculations using TDDFT and the CAM-factor were unsatisfactory for describing the observed electronic absorption spectra. Transitions into lower electronic states ($S_1 \leftarrow S_0$, $S_2 \leftarrow S_0$) had practically zero intensity. The $S_1 \leftarrow S_0$-transition experienced

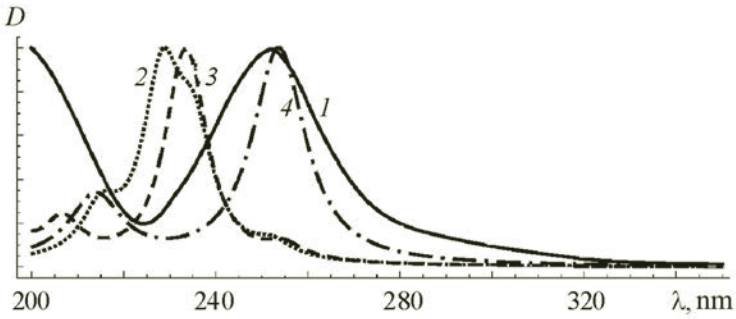

Fig. 3. Experimental (1) and calculated [TDDFT/CAM-B3LYP/cc-pVDZ (2); TDDFT/CAM-B3LYP/cc-pVDZ+SMD (EtOH) (3); and CASSCF(2,4)/XMCQDPT2 (4)] electronic absorption spectra of the studied compound.

TABLE 2. Bond Lengths (λ) and Oscillator Strengths (*f*) of Electronic Transitions of 3-(Adamantan-1-yl)-4-ethyl-1-[(4-phenylpiperazin-1-yl)methyl]-1*H*-1,2,4-triazole-5(4*H*)-thione Calculated at Various Theory Levels

Transition	TDDFT				CASSCF(2,4)/XMCQDPT2	
	CAM-B3LYP/cc-pVDZ		CAM-B3LYP/cc-pVDZ + SMD (EtOH)			
	λ, nm	*f*	λ, nm	*f*	λ, nm	*f*
$S_1 \leftarrow S_0$	272	0.001	263	0.003	254	0.795
$S_2 \leftarrow S_0$	252	0.028	255	0.045	214	0.245
$S_3 \leftarrow S_0$	235	0.215	235	0.283	156	0.374
$S_4 \leftarrow S_0$	228	0.337	232	0.411	101	0.001

TABLE 3. Greatest Biological Activities of 3-(Adamantan-1-yl)-4-ethyl-1-[(4-phenylpiperazin-1-yl)methyl]-1*H*-1,2,4-triazole-5(4*H*)-thione Predicted Based on Compound Structure

Pa	*Pi*	Activity
0.590	0.037	Proteasome ATP-ase inhibitor
0.496	0.003	11β-Hydroxysteroid dehydrogenase inhibitor
0.487	0.044	Analgesic
0.459	0.047	Polarization stimulator
0.438	0.008	α-Adrenoreceptor antagonist
0.412	0.067	Muramoyltetrapeptide carboxypeptidase inhibitor

a hypsochromic shift of 9 nm if the solvent was considered. It was supposed that errors in the TDDFT calculations were responsible for the ICT in the studied compound.

Figure 4 shows the upper "frozen" (doubly occupied) and four active molecular orbitals (MOs) from the total active space and also their occupancy factors (second, third, and fourth active MOs had the same occupancy factor). Figure 4 shows that the electron density shifted upon excitation partially from the piperazine and phenyl groups to the triazole ring although it was mostly localized on the S atom. Thus, the phenyl and piperazine rings in the studied compound acted as electron-density donors; the triazole, as an acceptor.

The wavelength of the $S_1 \leftarrow S_0$-transition that was calculated in the CASSCF(2,4)/XMCQDPT2 approximation [34] was 254 nm. The transition had a high intensity (Table 2; Fig. 3, curve 4). Thus, the electronic absorption spectrum of the studied compound that was calculated in terms of the multi-reference perturbation theory method agreed fully with the experimental data.

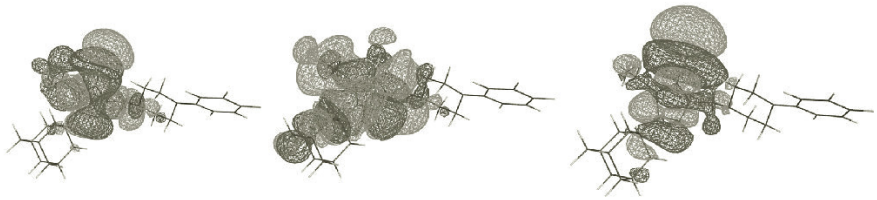

Second, third, and fourth active MOs (0.286)

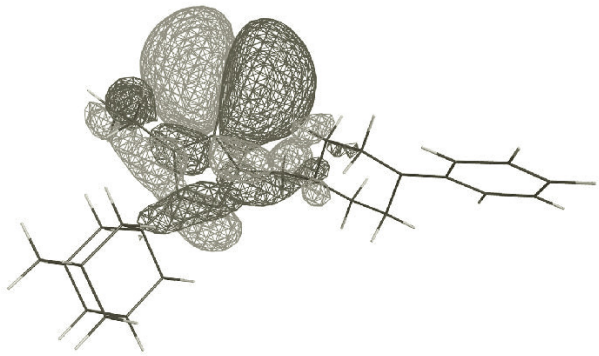

First active MO (1.142)

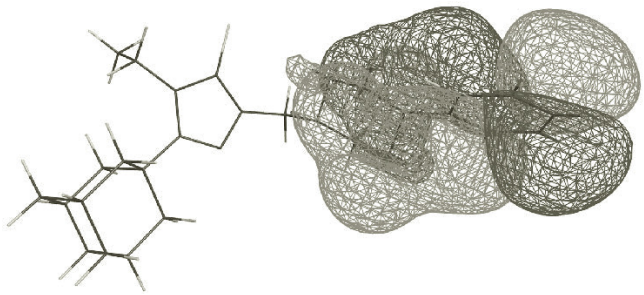

Second doubly occupied MO (2.000)

Fig. 4. Higher occupied MO, four active MOs, and their occupancy factors calculated in the CASSCF(2,4) approximation.

Biological activities. Table 3 presents the biological activity indices of the studied compound (i.e., the probability of activity *Pa* or inactivity *Pi* of the determined type) that were found using the PASS Online database [37]. According to the literature [36], if $Pa > 0.7$, then the examined compound will most probably demonstrate this activity experimentally. If $0.5 < Pa < 0.7$, then the compound may demonstrate experimental activity but the probability of this is less. If $Pa < 0.5$, the likelihood of this compound demonstrating this activity is low. According to Table 3, the studied compound probably acted as a proteasome ATP-ase inhibitor.

Conclusions. Spectral characteristics of 3-(adamantan-1-yl)-4-ethyl-1-[(4-phenylpiperazin-1-yl)methyl]-1*H*-1,2,4-triazole-5(4*H*)-thione, an adamantane-containing compound that is promising for drug development, were analyzed systematically. Vibrational IR and Raman spectra of the crystalline compound were interpreted based on quantum-chemical simulation in the B3LYP/cc-pVDZ approximation. Biological activity indices of the molecule were predicted based on the molecular structure and established that the studied compound was likely to act as a proteasome ATP-ase inhibitor. Simulation of the UV/Vis absorption spectrum using TDDFT and *ab initio* perturbation theory demonstrated that the first approximation was inadequate for describing the experimental spectrum of the studied compound. This was most likely a consequent of ICT. The calculations in the second of the aforementioned approximations agreed with the experimental data. The results could be used in medicinal chemistry and for analytical purposes.

Acknowledgment. The work was financially supported in part by the Deanship of Scientific Research at Princess Nourah bint Abdulrahman University through the Research Group Program (No. RGP-1438-0010).

REFERENCES

1. G. Lamoureux and G. Artavia, *Curr. Med. Chem.*, **17**, 2967–2978 (2010).
2. J. Liu, D. Obando, V. Liao, T. Lifa, and R. Codd, *Eur. J. Med. Chem.*, **46**, 1949–1963 (2011).
3. G. Ali Mansoori, P. L. Barros de Araujo, and E. Silvano de Araujo, *Diamondoid Molecules: With Applications in Biomedicine, Materials Science, Nanotechnology & Petroleum Science*, World Scientific Publishing (2012).
4. F. G. Hayden, *Antiviral Res.*, **71**, 372–378 (2006).
5. M.-J. Perez-Perez, J. Balzarini, M. Hosoya, E. De Clercq, and M.-J. Camarasa, *Bioorg. Med. Chem. Lett.*, **2**, 647–648 (1992).
6. I. Stylianakis, A. Kolocouris, N. Kolocouris, G. Fytas, G. B. Foscolos, E. Padalko, J. Neyts, and E. De Clercq, *Bioorg. Med. Chem. Lett.*, **13**, 1699–1703 (2003).
7. N. A. Ilyushina, N. V. Bovin, R. G. Webster, and E. A. Govorkova, *Antiviral Res.*, **70**, 121–131 (2006).
8. G. Zoidis, C. Fytas, I. Papanastasiou, G.B. Foscolos, G. Fytas, E. Padalko, E. De Clercq, L. Naesens, J. Neyts, and N. Kolocouris, *Bioorg. Med. Chem.*, **14**, 3341–3348 (2006)
9. A. A. El-Emam, O. A. Al-Deeb, M. A. Al-Omar, and J. Lehmann, *Bioorg. Med. Chem.*, **12**, 5107–5113 (2004).
10. M. Protopopova, C. Hanrahan, B. Nikonenko, R. Samala, P. Chen, J. Gearhart, L. Einck, and C. A. Nacy, *J. Antimicrob. Chemother.*, **56**, 968–974 (2005).
11. A. A. El-Emam, A.-M. S. Al-Tamimi, M. A. Al-Omar, K. A. Alrashood, and E. E. Habib, *Eur. J. Med. Chem.*, **68**, 96–102 (2013).
12. A. A. Kadi, E. S. Al-Abdullah, I. A. Shehata, E. E. Habib, T. M. Ibrahim, and A. A. El-Emam, *Eur. J. Med. Chem.*, **45**, 5006–5011 (2010).
13. K. Omar, A. Geronikaki, P. Zoumpoulakis, C. Camoutsis, M. Sokovic, A. Ciric, and J. Glamoclija, *Bioorg. Med. Chem.*, **18**, 426–432 (2010).
14. A. A. Kadi, N. R. El-Brollosy, O. A. Al-Deeb, E. E. Habib, T. M. Ibrahim, and A. A. El-Emam, *Eur. J. Med. Chem.*, **42**, 235–242 (2007).
15. E. S. Al-Abdullah, H. H. Asiri, S. Lahsasni, E. E. Habib, T. M. Ibrahim, and A. A. El-Emam, *Drug Des., Dev. Ther.*, **8**, 505–518 (2014).
16. O. Kouatly, A. Geronikaki, C. Kamoutsis, D. Hadjipavlou-Litina, and P. Eleftheriou, *Eur. J. Med. Chem.*, **44**, 1198–1204 (2009).
17. O. A. Al-Deeb, M. A. Al-Omar, N. R. El-Brollosy, E. E. Habib, T. M. Ibrahim, and A. A. El-Emam, *Arzneim. Forsch./Drug Res.*, **56**, 40–47 (2006).
18. S. Riganas, I. Papanastasiou, G. B. Foscolos, A. Tsotinis, J.-J. Bourguignon, G. Serin, J.-F. Mirjolet, K. Dimas, V. N. Kourafalos, A. Eleutheriades, V. I. Moutsos, H. Khan, S. Georgakopoulou, A. Zaniou, M. Prassa, M. Theodoropoulou, S. Pondiki, and A. Vamvakides, *Bioorg. Med. Chem.*, **20**, 3323–3331 (2012).
19. A. A. El-Emam, E. S. Al-Abdullah, H. M. Al-Tuwaijri, M. Said-Abdelbaky, and S. Garcia-Granda, *Acta Crystallogr., Sect. E: Struct. Rep. Online*, **68**, o2380–o2381 (2012).
20. M. B. Shundalau, E. S. Al-Abdullah, E. V. Shabunya-Klyachkovskaya, A. V. Hlinisty, O. A. Al-Deeb, A. A. El-Emam, and S. V. Gaponenko, *J. Mol. Struct.*, **1115**, 258–266 (2016).
21. A. M. Andrianov, I. A. Kashyn, V. M. Andrianov, M. B. Shundalau, A. V. Hlinisty, S. V. Gaponenko, E. V. Shabunya-Klyachkovskaya, A. Matsukovich, A.-M. S. Al-Tamimi, and A. A. El-Emam, *J. Chem. Sci.*, **128**, 1933–1942 (2016).
22. M. Shundalau, Y. Mindarava, A. Matsukovich, S. Gaponenko, and A. A. El-Emam, in: *Abstracts of the XIVth International Conference on Molecular Spectroscopy (ICMS2017)*, Bialka Tatrzanska, Poland (2017), p. 136.
23. M. W. Schmidt, K. K. Baldridge, J. A. Boatz, S. T. Elbert, M. S. Gordon, J. H. Jensen, S. Koseki, N. Matsunaga, K. A. Nguyen, S. J. Su, T. L. Windus, M. Dupuis, and J. A. Montgomery, Jr., *J. Comput. Chem.*, **14**, 1347–1363 (1993).
24. B. M. Bode and M. S. Gordon, *J. Mol. Graphics Modell.*, **16**, 133–138 (1998).
25. L. J. Farrugia, *J. Appl. Crystallogr.*, **30**, 565 (1997).
26. T. H. Dunning, Jr., *J. Chem. Phys.*, **90**, 1007–1023 (1989).
27. A. D. Becke, *J. Chem. Phys.*, **98**, 5648–5652 (1993).
28. C. Lee, W. Yang, and R. G. Parr, *Phys. Rev. B: Condens. Matter Mater. Phys.*, **37**, 785–789 (1988).
29. P. J. Stephens, F. J. Devlin, C. F. Chabalowski, and M. J. Frisch, *J. Phys. Chem.*, **98**, 11623–11627 (1994).
30. E. Runge and E. K. U. Gross, *Phys. Rev. Lett.*, **52**, 997–1000 (1984).
31. K. Burke, J. Werschnik, and E. K. U. Gross, *J. Chem. Phys.*, **123**, 062206 (2005).

32. T. Yanai, D. P. Tew, and N. C. Handy, *Chem. Phys. Lett.*, **393**, 51–57 (2004).
33. A. V. Marenich, C. J. Cramer, and D. G. Truhlar, *J. Phys. Chem. B*, **113**, 6378–6396 (2009).
34. A. A. Granovsky, *J. Chem. Phys.*, **134**, 214113 (2011).
35. Alex A. Granovsky, Firefly version 8; http://classic.chem.msu.su/gran/firefly/index.html.
36. A. Lagunin, A. Stepanchikova, D. Filimonov, and V. Poroikov, *Bioinformatics*, **16**, 747–748 (2000).
37. PASS Online; http://way2drug.com/passonline/index.php.
38. G. A. Pitsevich, M. B. Shundalau, M. A. Ksenofontov, and D. S. Umreiko, *Global J. Anal. Chem.*, **2**, 114–124 (2011).
39. V. Arjunan, T. Rani, C. V. Mythili, and S. Mohan, *Spectrochim. Acta, Part A*, **79**, 486–496 (2011).
40. I. Hargittai and K. Hedberg, in: *Molecular Structures and Vibrations*, S. J. Cyvin (Ed.), Elsevier Publishing Co., New York (1972), pp. 340–357.
41. N. W. Larsen, *J. Mol. Struct.*, **51**, 175–190 (1979).
42. S. Gunasekaran and B. Anita, *Indian J. Pure Appl. Phys.*, **46**, 833–838 (2008).
43. K. Kuchitsu (Ed.), *Structure of Free Polyatomic Molecules. Basic Data*, Springer (1998).
44. L. Bistricic, G. Baranovic, and K. Mlinaric-Majerski, *Spectrochim. Acta, Part A*, **51**, 1643–1664 (1995).
45. E. I. Bagrii, *Adamantanes: Preparation, Properties, Applications* [in Russian], Nauka, Moscow (1989).
46. R. M. Silverstein, F. X. Webster, and D. J. Kiemle, *Spectrometric Identification of Organic Compounds*, 7th edn., Wiley & Sons, Inc., (2005).
47. L. Goodman, A. G. Ozkabak, and S. N. Thakur, *J. Phys. Chem.*, **95**, 9044–9058 (1991).
48. P. J. Hendra and D. B. Powell, *Spectrochim. Acta*, **18**, 299–306 (1962).
49. O. Alver, C. Parlak, and M. Şenyel, *Spectrochim. Acta, Part A*, **67**, 793–801 (2007).
50. S. A. Kudchadker and C. N. R. Rao, *Indian J. Chem.*, **11**, 140–142 (1973).
51. F. Billes, H. Endredi, and G. Keresztury, *J. Mol. Struct.: THEOCHEM*, **530**, 183–200 (2000).